Journal of Comparative Pathology 216 (2025) 1–9

Contents lists available at ScienceDirect

Journal of Comparative Pathology

journal homepage: www.elsevier.com/locate/jcpa

Spontaneously arising disease

Morphometry, cellular characterization and temporal evolution of granulomas induced by aluminium oxyhydroxide in sheep

Ana Rodríguez-Largo [a], Álex Gómez [a, b], Estela Pérez [a, b], Ricardo de Miguel [a, 1], Irati Moncayola [c], Lucia Biagini [d], Giacomo Rossi [d], Ignacio de Blas [a, b], Antonio Fernández [a, b], Marta Pérez [b, e], Idoia Glaria [c], Ramsés Reina [c], Lluís Luján [a, b, *]

[a] Departamento de Patología Animal, Universidad de Zaragoza, 50013 Zaragoza, Spain
[b] Instituto Universitario de Investigación Mixto Agroalimentario de Aragón (IA2), Universidad de Zaragoza, 50013 Zaragoza, Spain
[c] Instituto de Agrobiotecnología, CSIC-Gobierno de Navarra, 31192 Mutilva, Spain
[d] Scuola di Bioscienze e Medicina Veterinaria, Università di Camerino, 62024 Matelica, Italy
[e] Departamento de Anatomía, Embriología y Genética, Universidad de Zaragoza, 50013 Zaragoza, Spain

ARTICLE INFO

Article history:
Received 3 July 2024
Accepted 8 November 2024

Keywords:
aluminium
granuloma
lentivirus
polarization
sheep
vaccine

ABSTRACT

Persistent subcutaneous granulomas form at the injection site following administration of aluminium oxyhydroxide (AlOOH), a widely used vaccine adjuvant. Small ruminant lentiviruses (SRLVs) can infect macrophages within granulomas induced by commercial AlOOH-based vaccines in sheep. The entry of SRLVs into target cells involves the mannose receptor (*MR*), while catalytic polypeptide-like 3 protein containing Z1 domain (*A3Z1*) is considered a restriction factor for lentiviral replication. The objective of this study was to investigate the temporal evolution of AlOOH-induced post-vaccination granulomas in sheep experimentally infected with SRLVs. Twenty-four male lambs underwent two identical vaccination protocols and were challenged with SRLVs. Granulomas were detected in vaccinated groups only and progressively decreased in size. At post-mortem examination, 91.3% of the granulomas were recovered. Fistulas were present in granulomas following the second vaccination protocol. Central necrosis was present in 58.0% of granulomas and was associated with the vaccine used. Orthokeratotic keratin was seen within granulomas in 47.1% of the lambs. Considering all granulomas studied, significantly higher expression of *MR* was found compared with *A3Z1*. Differences in *MR* expression were related to the type of vaccine and the time since vaccination. *A3Z1* expression was upregulated in granulomas from the infected groups. Macrophage polarization may influence SRLV infection of granulomas. While SRLV infection does not influence the architecture of post-vaccination granulomas, it may modulate their immune microenvironment. Further studies are needed to elucidate the complex interactions between AlOOH-induced granulomas and SRLV infection in sheep.

1. Introduction

Adjuvants induce, enhance and maintain specific immune responses against inactivated antigens in vaccines [1]. Aluminium oxyhydroxide (AlOOH) is one of the most widely used adjuvants in licensed human and veterinary vaccines [2], yet its basic mechanism of action is poorly understood [3]. AlOOH is known to activate innate and adaptive immune cells, leading to a Th2 biased response to vaccine antigens [3], and it can upregulate the expression of antigen-presenting and co-stimulatory molecules on cells of monocyte–macrophage lineage by an interleukin-4-dependent mechanism [4,5]. Internalized AlOOH can damage lysosomal membranes, triggering cathepsin-mediated cell death [6]. The cytotoxic effects of AlOOH activate the immune system through damage-associated molecular patterns (DAMPs), such as uric acid [7] and DNA [8]. Furthermore, this adjuvant promotes the recruitment of antigen-presenting cells (APCs) to the injection site and their systemic biodistribution [9–11].

Sheep health programmes include vaccination to prevent and control infectious diseases [12]. Consequently, multiple vaccines

* Corresponding author.
E-mail address: Lluis.Lujan@unizar.es (L. Luján).
[1] Current affiliation of Ricardo de Miguel is Anapath Services GmbH, Hammerstrasse 49, 4410 Liestal, Switzerland.

https://doi.org/10.1016/j.jcpa.2024.11.002

are often administered to a single animal each year depending on production targets, disease prevalence and geographical region [13]. The administration of AlOOH-based vaccines in sheep induces granulomas at the injection site, consisting of macrophages and fewer multinucleated giant cells (MGCs), lymphocytes and neutrophils [14]. AlOOH particles can persist at the injection site and be systemically distributed to distant tissues, including regional lymph nodes and the central nervous system [14,15].

Macrophages are plastic cells that display diverse phenotypes and functional responses under specific stimuli [16]. Two major pathways of macrophage activation are recognized: classically activated macrophages (M1) that promote inflammation and, alternatively activated macrophages (M2) that are involved in the resolution of inflammation [17,18]. Macrophage polarization is a key factor in the outcomes of infectious diseases caused by different pathogens, including porcine arteriviruses (eg, porcine reproductive and respiratory syndrome virus) [19], human lentiviruses (eg, human immunodeficiency virus) [20], small ruminant lentiviruses (SRLVs) [21] and ruminant mycobacteria [22–24].

In sheep, M1-like stimuli may enhance the expression of interferon-induced restriction factors, such as the apolipoprotein B mRNA editing enzyme, catalytic polypeptide-like 3 (APOBEC3), while M2-like stimuli are associated with the upregulation of mannose receptor (*MR*) and dendritic cell-specific intercellular adhesion molecule-3-grabbing non-integrin (*DC-SIGN*) [21]. APOBEC3 proteins containing Z1 domain (*A3Z1*) are restriction factors highly expressed in SRLV-resistant cells, such as monocytes and M1 macrophages [25]. In contrast, the *MR* expressed on M2 macrophages is proposed to be a key mediator for SRLV entry to target cells and tissue distribution [21,26]. Therefore, macrophage polarization in AlOOH-induced granulomas may influence SRLV infection and replication. Most knowledge about the polarization of SRLV-infected cells has come from in-vitro studies of blood monocyte-derived macrophages [21,25–27], with no information available on this process in in-vivo developed post-vaccination granulomas.

SRLVs cause progressive multisystemic inflammatory disease [28], directly affecting the welfare, production [29,30] and global trade of small ruminants [31]. The main target organs of SRLVs include the lungs, central nervous system, joints and mammary gland [32]. Currently, there are no treatments or vaccines to control SRLV infection, and attempts to develop an effective vaccine have failed [33]. However, SRLVs can infect granulomas induced by commercial AlOOH-based vaccines against various ovine pathogens, such as *Clostridium* spp, bluetongue virus and *Chlamydia abortus* [34].

Granuloma formation is a constant finding after AlOOH-based vaccine injections in sheep [35]. However, there is a notable knowledge gap regarding their evolution, cellular composition and potential interactions with infectious pathogens. The aim of this study was to investigate the temporal evolution of AlOOH-induced post-vaccination granulomas in lambs experimentally infected with SRLVs and to provide insights into factors that may influence their morphometry and composition, including SRLV infection.

2. Material and methods

2.1. Animals and experimental groups

The experimental design and all procedures were approved by the Ethical Committee of the University of Zaragoza (PI42/18) and conducted in accordance with Spanish Policy (Royal Decree 53/2013), which implements Directive 2010/63/EU of the European Parliament for the protection of animals used for scientific purposes. Twenty-four male Rasa Aragonesa lambs were sourced from a long-term SRLV-seronegative flock ('Masía El Chantre', Spain). Newborn lambs and their ewes were kept in isolated pens and their seronegative status was confirmed with three commercial ELISA tests: (1) Eradikit SRLV Screening kit (In3Diagnostic, www.in3diagnostic.com); (2) Elitest MVV/CAEV (Hyphen Biomed, www.hyphen-biomed.com); and (3) INgezim Maedi screening (Eurofins Technologies Ingenasa, www.eurofins.com). Three-month-old post-weaned lambs were housed at the experimental facilities of the University of Zaragoza and divided into five treatment groups. At 6 months, the animals underwent an experimental protocol involving the subcutaneous administration of two commercial AlOOH-based vaccines or a saline solution, combined with a challenge with SRLVs or uninfected culture medium (Table 1).

2.2. Study design: vaccination schedule and small ruminant lentivirus challenge

All lambs in the vaccinated groups (1, 3 and 5) received two different commercial AlOOH-based vaccines: vaccine 1 against bluetongue virus and vaccine 2 against members of the Pasteurellaceae and Clostridiaceae families (Supplementary Table 1). The first vaccination protocol included a 2 ml dose of each vaccine at 0 days post treatment (dpt) and again at 30 dpt. This protocol was repeated at 135 and 165 dpt, resulting in each lamb receiving a total of eight vaccine doses (Supplementary Fig. S1). Lambs in each control group (2 and 4) received an identical number and volume of saline solution injections on the same dates. The anatomical locations of the injections are detailed in Supplementary Fig. 2.

The challenge with the previously used SRLVs strain ov496 [36] was carried out after completion of the first vaccination schedule, at 36 dpt. The same protocol was repeated at 93 dpt to ensure infection of the lambs (Supplementary Fig. 1). A total of 10^6 tissue culture infectious dose ($TCID_{50}$) per animal was inoculated either intravenously (IV) or intratracheally (IT), depending on the group (Table 1). Lambs in group 5 were inoculated via the IT (n = 3) or IV (n = 3) route with non-infected culture medium (Gibco Dulbecco's Modified Eagle Medium [DMEM]; Thermo Fisher Scientific, www.thermofisher.com). Two animals, one from group 2 and one from group 5, died due to anaesthesia during the IT infection procedure. Therefore, a total of 22 lambs completed the study, which lasted about 8.5 months.

2.3. In-vivo studies

The evaluation of morphometric changes in AlOOH-induced post-vaccination granulomas was based on shape, as well as length and width measurements obtained with an automated calliper at 7, 16 and 35 days after injection. Due to the ellipse-like shape of the

Table 1
Experimental design

Groups	n	Vaccines/control	Viral challenge/ control	Viral infection route
Group 1 AlOOH vaccines and SRLV IT	6	AlOOH vaccines	SRLV	IT
Group 2 SRLV IT only	2	Saline solution	SRLV	IT
Group 3 AlOOH vaccines and SRLV IV	6	AlOOH vaccines	SRLV	IV
Group 4 SRLV IV only	3	Saline solution	SRLV	IV
Group 5 AlOOH vaccines only	5	AlOOH vaccines	Non-infected culture medium	IT or IV

AlOOH, aluminium oxyhydroxide; IT, intratracheal; IV, intravenous; n, number of lambs per group at end of experiment; SRLV, ov496 strain of small ruminant lentivirus.

post-vaccination granulomas, Ramanujan's formula ($P \approx \pi [3 (a+b) - \sqrt{((3 a+b) (a+3 b))}]$) was used to estimate the perimeter [37].

2.4. Post-mortem studies

Lambs were humanely killed with an overdose of IV pentobarbital and a complete necropsy was performed. However, this report focuses exclusively on the post-vaccination granulomas. During the experiment, nine granulomas were biopsied (results to be described elsewhere) and only 127 out of 136 granulomas were expected to be detected at post-mortem examination. Animals were placed in lateral recumbency, the granulomas were located by palpation and the presence of fistulas was recorded. Skin and adipose tissue were removed to expose the subcutaneous tissue, and all post-vaccination granulomas found were sampled. Sections of each granuloma were trimmed and fixed in 10% neutral-buffered formalin, while a selection of granulomas (n = 50, Supplementary Table 2) were collected for molecular studies by immersion in RNAlater solution (Thermo Fisher Scientific) and stored at −20°C until processing. Formalin-fixed samples were routinely processed through graded alcohols, embedded in paraffin wax and 4 μm sections cut for haematoxylin and eosin (HE) staining and immunohistochemical procedures.

2.5. Pathological studies

Histological characterization of AlOOH-induced granulomas was based on a modified semiquantitative scoring system [14], as detailed in Supplementary Table 3. Immunohistochemical studies employed the avidin–biotin–peroxidase complex method (Vectastain Elite ABC Kit; Vector Laboratories, https://vectorlabs.com) with 3,3′-diaminobenzidine (Vector Laboratories) as chromogen. Details of the primary antibodies and technical aspects are summarized in Table 2. In brief, sections were subjected to specific pretreatments for antigen retrieval. Non-specific binding sites were blocked by incubating sections at room temperature for 1 h with normal serum, obtained from the species corresponding to the secondary antibody, diluted in a solution of 1% polyvinylpyrrolidone, 1% bovine serum albumin and 1% tris-buffered saline (PVP-BSA-TBS). Ionized calcium-binding protein molecule 1 (Iba1) antibody, a pan-macrophage marker, was used for all granulomas (n = 112). For T lymphocytes (anti-CD3) and viral (anti-p28) detection, two granulomas from four different lambs in each vaccinated group (1, 3 and 5, n = 24) were investigated as described [38–40]. Ovine lymph nodes were used as positive controls for Iba1 and CD3 analyses, while SRLV-affected lungs were used for p28 detection. Granulomas from group 5 were included as SRLV-negative controls. The specificity of the technique was demonstrated by replacing the primary antibody with PVP-BSA-TBS solution and, in previous studies, by using isotype-matched antibodies against irrelevant antigens [38–40].

2.6. Relative target gene expression in granulomas

Twenty mg of each granuloma were homogenized using steel beads in a vibration grinding mill (Mikro-Dismembrator U; Sartorius AG, www.sartorius.com), followed by RNA extraction and purification using a magnetic bead-based method (NucleoMag RNA-MagnetaPure32; MACHEREY-NAGEL, www.mn-net.com). The quantity and purity of the extracted nucleic acids were evaluated with a microvolume ultraviolet-visible spectrophotometer (NanoDrop One/One; Thermo Fisher Scientific). A total of 1,000 ng of RNA was retrotranscribed into cDNA using the PrimeScript RT Reagent kit (Takara Bio, www.takarobio.com) with a single thermal cycle at 37°C for 15 min, followed by a cycle at 85°C for 15 s. Quantitative analyses of target genes (*A3Z1*, *DC-SIGN* and *MR*) were conducted in a total volume of 25 μl, using 5 μl of cDNA, DNA-binding dye (SYBR Green Master Mix; Bio-rad, www.biorad.com) and specific primers previously used in sheep samples [21]. β-actin was used as the housekeeping gene and no template controls were included in each run. Quantitative polymerase chain reactions (qPCRs) and data analyses were performed using the AriaMx Real-time PCR System (Agilent Technologies, www.agilent.com). Relative mRNA quantifications were determined by subtracting the β-actin Ct value from the target gene Ct value in each sample (ΔCt) and were expressed as $2^{-\Delta Ct}$ value [41].

2.7. Statistical analyses

Quantitative variables (eg, perimeter of granulomas and relative target gene expression) were tested for normality and equality of variance using the Shapiro–Wilk test and Levene's test, respectively. Unpaired comparisons between categorical variables with three or more categories (eg, treatment group) were analysed with the Kruskal–Wallis test, followed by Dunn's test as post-hoc test (non-normally distributed data). For variables with two categories (eg, type of vaccine), comparisons were performed using the Mann–Whitney U test (non-normally distributed data) or Student's t-test (normally distributed data). Paired comparisons within each categorical variable between sampling dates were carried out with the Wilcoxon test (non-normally distributed data) or Student's t-test (normally distributed data) [42]. Detection of fistulas and microscopic features were coded as binary variables (0 and 1, representing presence [P] and absence [A], respectively). The P/A of these variables was described using relative frequencies. Associations between qualitative and categorical variables were analysed using Pearson's Chi-square test; alternatively, Fisher's exact probability test was applied for 2 × 2 contingency tables and Likelihood Ratio test for the rest of the cases [43]. Data were analysed using SPSS Statistics 26.0 software (IBM Corporation, www.ibm.com), with a *P* value <0.05 considered statistically significant. Graphs were created by GraphPad Prism version 8.0 software (GraphPad, www.graphpad.com).

Table 2
Antibodies used for immunolabelling of aluminium oxyhydroxide-induced post-vaccination granulomas in experimental lambs

Antibody	Host	Type	Pre-treatment	Dilution	Incubation	Source
Anti-p28 (clone CAEP5A1)	Mouse	M	Microwave, citrate buffer, pH6	1:400	Overnight (room temperature)	VMRD (www.vmrd.com)
Anti-CD3	Rabbit	P	Pressure cooker, citrate buffer, pH6	1:100	Overnight (4°C)	Agilent Dako (www.agilent.com)
Anti-Iba1	Rabbit	P	Microwave, citrate buffer, pH6	1:300	Overnight (4°C)	FUJIFILM Wako Pure Chemical Corporation (www.fugifilm.com)

M, monoclonal; P, polyclonal.

3. Results

3.1. Morphometric evolution of granulomas

Post-vaccination granulomas were detected only in the vaccinated groups (1, 3 and 5) as well-demarcated, soft and mobilizable subcutaneous nodules. Granulomas were absent in the groups (2 and 4) injected with saline solution. A significant (P <0.050) and progressive decrease in granuloma size was seen during the first 35 days post vaccination, independent of the type of vaccine (Fig. 1). However, granulomas induced by vaccine 2 had a significantly greater mean perimeter than those induced by vaccine 1 at 7, 16 and 35 days post vaccination (Fig. 1). Only subtle differences in granuloma shape were seen; most granulomas that developed following vaccine 1 were plaque-like, while those from vaccine 2 tended to bulge from the skin (Fig. 2A).

3.2. Pathological characterization

In-vivo evaluation of injection sites revealed minimal macroscopic changes associated with AlOOH-induced granulomas; the skin over some granulomas was alopecic (Fig. 2A) and/or exhibited a communication with the outer skin (fistula) (Fig. 2A inset). A total of 116 out of 127 post-vaccination granulomas (91.3%) were recovered from the subcutaneous tissue at post-mortem examination (Fig. 2B). At this time, fistulas were observed in nine out of 116 (7.8%) granulomas. Presence of fistulas was associated ($P = 0.012$, Fisher exact test) with vaccine type, being predominantly found in granulomas induced by vaccine 2 (8/9; 88.9%) compared with vaccine 1 (1/9; 11.1%). All fistulas (9/9) occurred in granulomas induced by the second vaccination protocol (at 135 and 165 dpt), with none observed after the first vaccination protocol (at 0 and 30 dpt).

For histopathological analyses, only 112 out of the 116 granulomas were evaluated, as four were minimally sized. AlOOH-induced granulomas were a highly cellular inflammatory reaction, primarily composed of epithelioid macrophages mixed with MGCs, surrounded by varying amounts of fibrous connective tissue. Over half of the AlOOH-induced granulomas (65/112; 58.0%) contained a variably sized area of central necrosis (Fig. 2C). Necrosis was associated ($P < 0.001$, Pearson's chi-square test) with the type of vaccine, occurring more frequently in granulomas from vaccine 1 (43/59; 72.9%) than from vaccine 2 (22/53; 41.5%). Foci of mineralization were observed in 35 out of 112 (31.3%) scattered throughout necrotic areas (Fig. 2C). Necrosis was also linked ($P = 0.007$, Pearson's chi-square test) to the presence of lymphoid aggregates but was independent of the time post vaccination ($P = 0.615$, Pearson's chi-square test). A total of 55 out of 112 (49.1%) granulomas contained lymphoid cells arranged in various patterns (Supplementary Fig. 3A–C): (i) linear groups parallel to necrotic areas, (ii) follicular-like structures, and (iii) random interspersion with macrophages. Two of these patterns often co-occurred in the same granuloma. No statistical association was found between the presence of lymphoid aggregates and the type of vaccine or dpt ($P = 0.127$ and $P = 0.438$, Pearson's chi-square test, respectively).

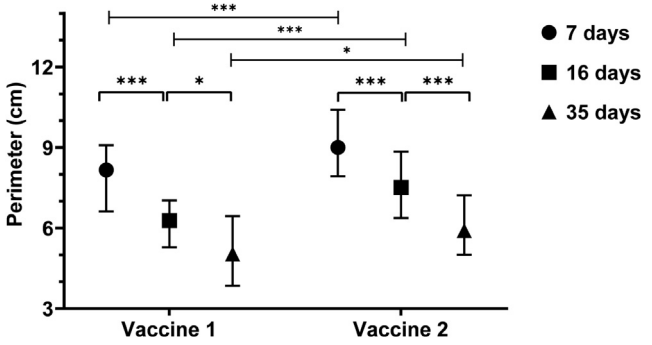

Fig. 1. Perimeter (cm) of post-vaccination granulomas following vaccines 1 and 2. Median values represented as circles (7 days post treatment, dpt), squares (16 dpt) and triangles (35 dpt). Whisker bars indicate interquartile range. *, statistical significance (P <0.05); ***, statistical significance (P <0.001).

Neutrophils were found in 25 out of 112 (22.3%) granulomas. Their presence was associated with dpt ($P = 0.046$, Pearson's chi-square test), being more common in granulomas formed at 135 and 165 dpt (18/61; 29.5%) compared with those at 0 and 30 dpt (7/51; 13.7%). The presence of neutrophils was also linked ($P = 0.008$, Pearson's chi-square test) to the type of vaccine, and these cells were found in a higher proportion of granulomas following vaccine 1 (19/59; 32.2%) compared with vaccine 2 (6/53; 11.3%). Scant to moderate layers of orthokeratotic keratin were seen between the granulomatous reaction and the necrotic content in nine out of 112 (8.0%) granulomas (Fig. 2D). Overall, eight out of 17 (47.1%) lambs had at least one granuloma with keratin. The presence of keratin was associated ($P = 0.004$, Fisher exact test) with dpt, as it was only found in 135 and 165 dpt granulomas. Keratin layers were occasionally lined by stratified squamous epithelium, with a small follicular-like cyst noted in one post-vaccination granuloma (Fig. 2D inset).

3.3. Immunohistochemical studies

Epithelioid macrophages and MGCs within granulomas had strong, membranous Iba1 labelling (Fig. 3A). CD3-positive lymphocytes exhibited cytoplasmic to membranous labelling and they were located at the periphery of the necrotic tissue (Fig. 3B) or formed lymphoid aggregates (Fig. 3C). SRLV protein was detected in the cytoplasm of macrophages and occasionally in MGCs of all examined granulomas from experimentally infected lambs, regardless of infection route (Fig. 3D). Granulomas from non-SRLV-infected lambs were consistently devoid of labelling.

3.4. Relative target gene expression in granulomas

MR expression was significantly higher (P <0.001) than *A3Z1* expression when granulomas from all vaccinated groups (1, 3 and 5) were considered. Differences in *A3Z1* expression were found between groups (Fig. 4A): *A3Z1* was significantly ($P = 0.020$) upregulated in granulomas from the infected group 3 compared with those from the non-infected group 5. Similarly, *A3Z1* was upregulated, albeit not significantly ($P = 0.064$), in granulomas from the infected group 1 compared with those from group 5. There were no differences in *A3Z1* expression between infected groups (1 and 3). Similarly, no significant differences in *A3Z1* expression were observed in granulomas induced by the two vaccines or at different dpt (Supplementary Fig. S4). *MR* expression in granulomas was similar between all groups (Fig. 4A). However, *MR* expression was significantly ($P = 0.020$) higher in granulomas induced at 135 dpt by vaccine 1 compared with those induced by vaccine 2, with no significant differences in granulomas induced at 0 dpt (Fig. 4B). As *DC-SIGN* expression was minimal, further analyses using this gene were not performed.

4. Discussion

This study provides new insights into the histopathological features of AlOOH-induced post-vaccination granulomas in sheep. Advancing our understanding of the mechanisms underlying these chronic inflammatory reactions and their interactions with

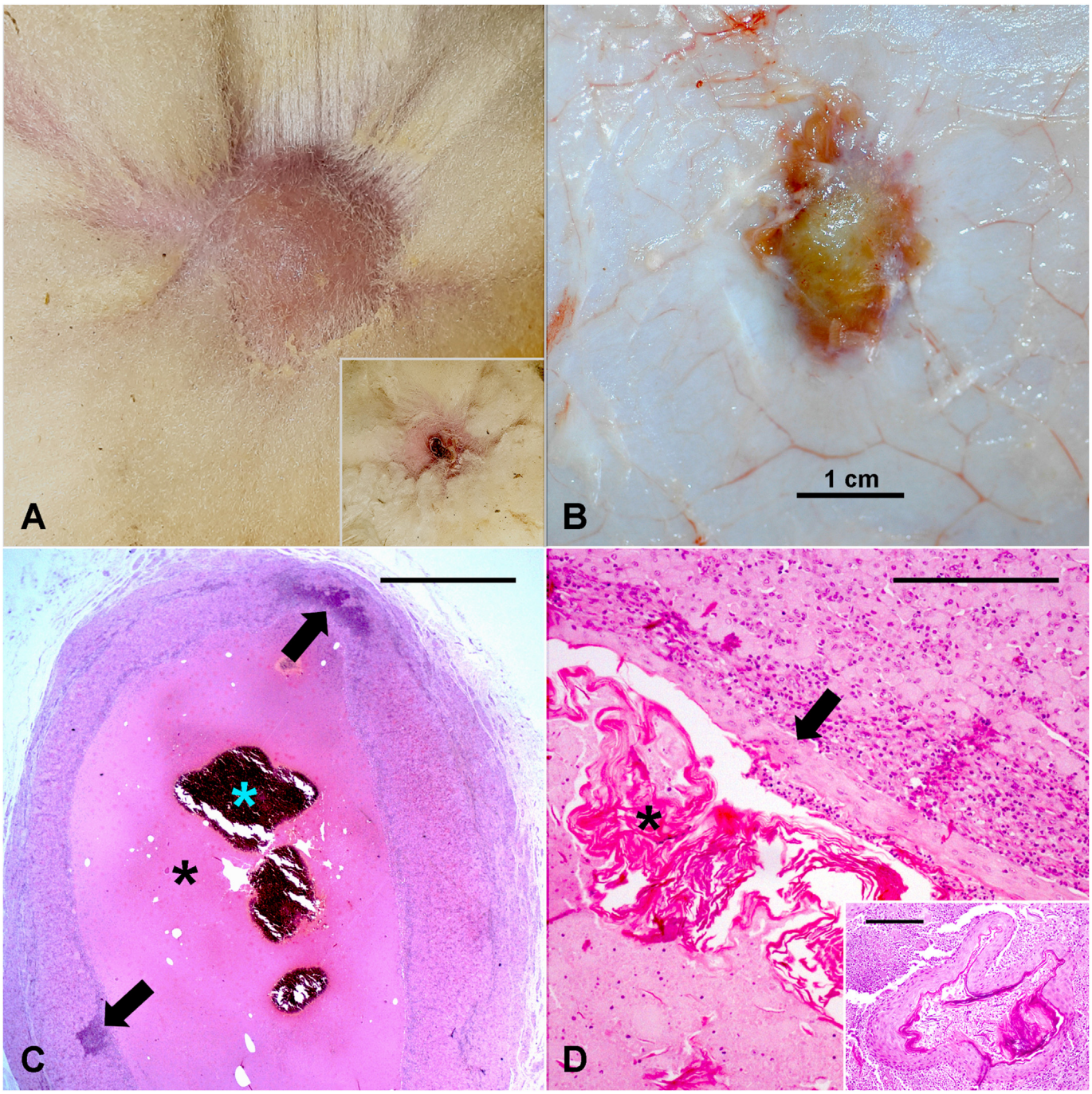

Fig. 2. Aluminium oxyhydroxide-induced post-vaccination granulomas, sheep. (**A**) In-vivo examination, vaccine 2. Well-demarcated, rounded and bulging granuloma (approximately 3–4 cm) covered by alopecic skin. Inset: fistula in a granuloma covered by a crust. (**B**) Post-mortem examination, vaccine 2. Granuloma in subcutaneous tissue following adipose tissue removal. (**C**) Granuloma architecture. Layers of macrophages with multifocal lymphoid aggregates (arrows) surrounding central necrotic area (black asterisk) with foci of mineralization (blue asterisk). HE. Bar, 300 μm. (**D**) Keratin layers (asterisk) lined by stratified epithelium (arrow) at periphery of necrotic area. HE. Bar, 300 μm. Inset: small follicular-like cyst in another granuloma. Bar, 500 μm.

lentiviruses is crucial, as granuloma formation is a constant local side effect following vaccination with AlOOH-based adjuvants.

In the present study, 91.3% of the expected granulomas were found at the end of the study, indicating a high persistence of these inflammatory reactions at the injection site. AlOOH-induced granulomas reached their maximum size at 7 days post vaccination, aligning with findings in mice in which inflammatory cell recruitment also peaked at this time [44]. The size reduction found in our study may be related to phagocytosis of AlOOH particles and their migration to distant sites, as reported in sheep [14,15], rabbits [45] and mice [10,11]. In our study, granulomas induced by vaccine 2 were larger and more conspicuous than those from vaccine 1, probably due to the nearly double AlOOH content in vaccine 2 (Supplementary Table 1). However, Asín *et al* [14] noted that in sheep, larger granulomas were induced by commercial vaccines containing longer aluminium particles compared with those induced by the injection of an equal amount of AlOOH alone. This finding suggests the probable influence of other factors such as the

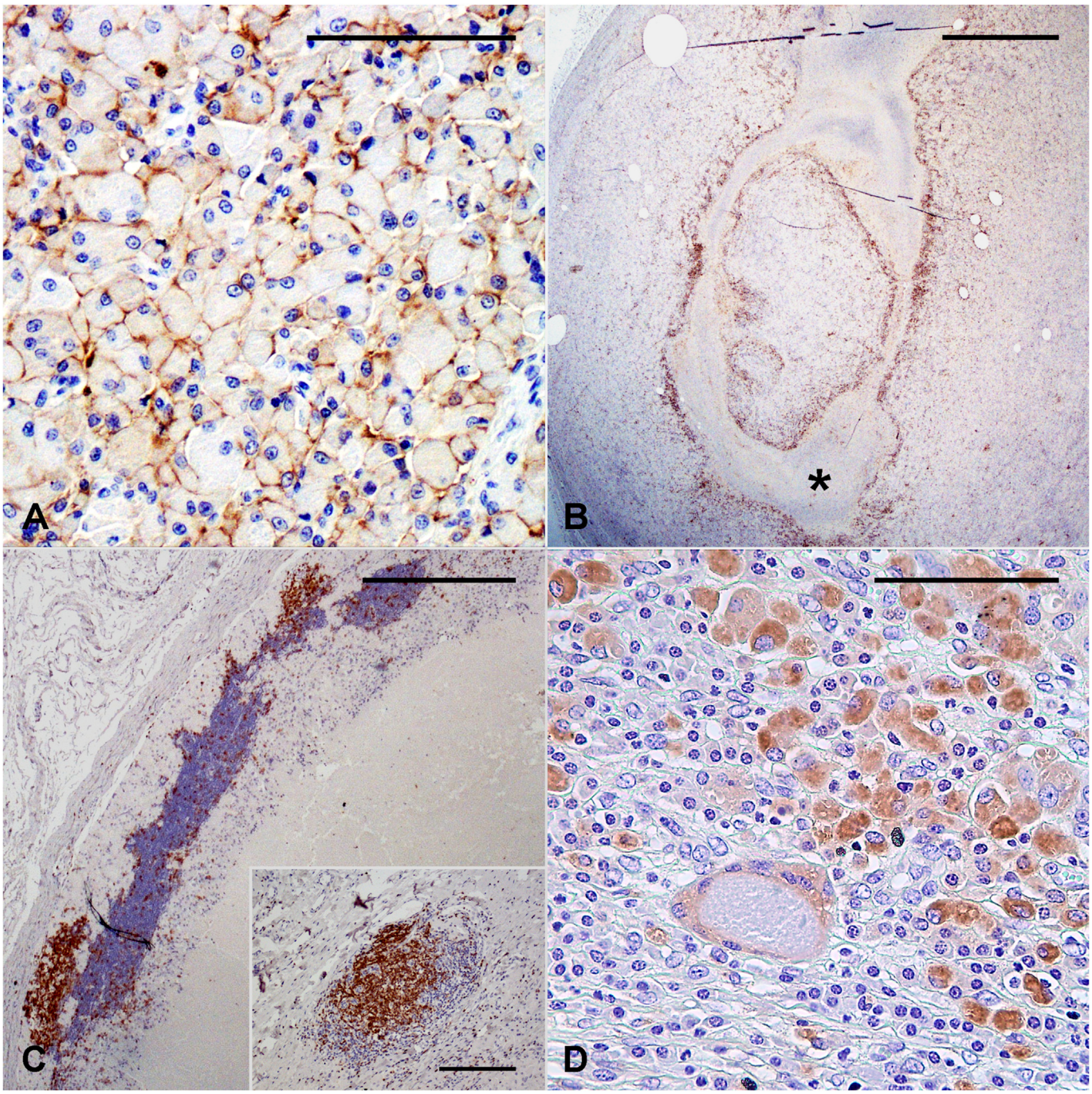

Fig. 3. Aluminium oxyhydroxide-induced post-vaccination granulomas, sheep, immunohistochemistry. (**A**) Iba1 immunolabelling of cell membranes of macrophages and multinucleated giant cell (MGCs). Bar, 50 μm. (**B**) Dense band of CD3-positive lymphocytes border necrotic area (asterisk). Bar, 300 μm. (**C**) CD3-positive lymphocyte aggregates at periphery of band of CD3-negative cells. Bar, 100 μm. Inset: follicular lymphoid aggregate mainly composed of CD3-positive lymphocytes. Bar, 500 μm (**D**) Granular to diffuse positive labelling for SRLV capsid protein p28 in cytoplasm of macrophages and MGCs. Bar, 50 μm.

physicochemical properties of AlOOH–antigen complexes [46] or the effects of other components in vaccine formulations on the morphometry of granulomas.

Fistulas were primarily seen in vaccine 2 granulomas, probably due to their larger size and increased pressure in the subcutis, which may favour the discharge of necrotic content to the exterior. While fistulation of post-vaccination granulomas has been reported in sheep [14], our results indicate it is an uncommon event, mainly occurring in the first months after granuloma formation. The presence of necrotic areas may be also linked to the physicochemical properties of the AlOOH–antigen complexes, rather than to higher AlOOH content, as they were more frequently found in granulomas induced by vaccine 1, which had a lower AlOOH concentration (Supplementary Table 1). Necrosis in granulomas was also associated with the presence of lymphoid aggregates. Indeed, AlOOH-induced cytotoxicity leads to the release of molecules recognized as DAMPs [7,8], which promote the activation of APCs and cytotoxic T lymphocytes, potentially driving so-called immunogenic cell death [47]. Neutrophils were more frequently seen in granulomas aged 3–4 months, declining thereafter, which

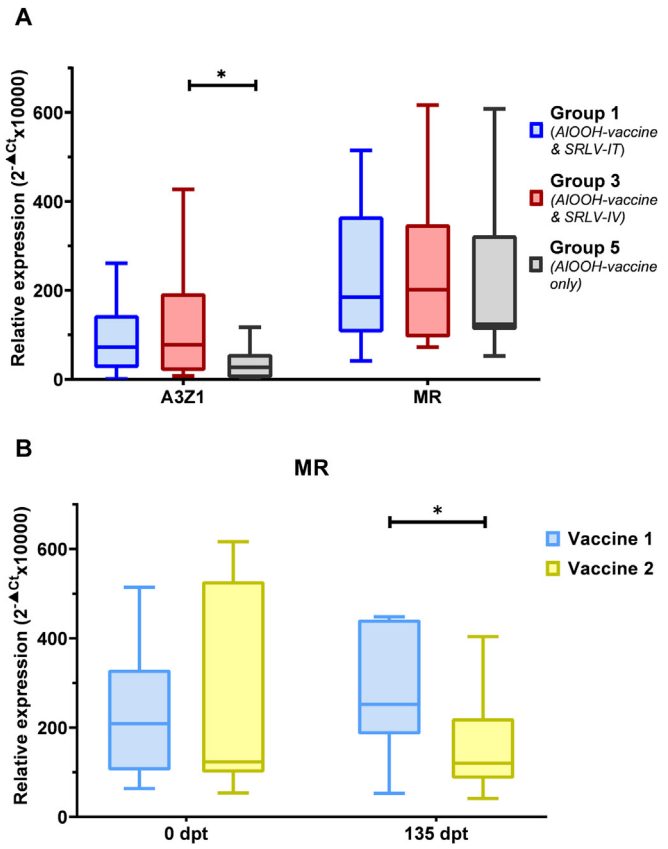

Fig. 4. Relative expression of target genes. (**A**) *APOBEC3Z1* (*A3Z1*) and mannose receptor (*MR*) expression in post-vaccination granulomas from vaccinated lambs. (**B**) *MR* expression in post-vaccination granulomas induced by vaccine 1 and vaccine 2 at 0 days post treatment (dpt) and 135 dpt. Data presented as $2^{-\Delta Ct} \times 10{,}000$ normalized to β-actin. Box plots represent median and quartiles, with whiskers indicating minimum and maximum values. *, statistical significance (P <0.050). SRLV-IT, SRLV administered by intratracheal route; SRLV-IV, SRLV administered by intravenous route.

aligns to observations in mice [44]. The presence of keratin constituted a novel finding in sheep, observed exclusively in granulomas aged 3–4 months. Skin trauma and/or the expansion of the granulomatous reaction may cause hair entrapment, potentially resulting in the formation of follicular cysts, as suggested in dogs, cats [48] and sheep [49]. Follicular cyst formation has been reported in rabbits following intradermal injections [50,51] and in humans after vaccination [52]. Remarkably, human pilomatrixomas have also been linked to vaccine injections [53–56]. Further research is required to determine whether post-vaccination granulomas in sheep influence the development of certain skin conditions.

Our results indicate that SRLV infection does not influence the cellular architecture of post-vaccination granulomas but may modulate their immune microenvironment. The upregulation of *MR* found in ovine AlOOH-induced granulomas suggests a polarization of macrophages toward an M2-like phenotype, which may favour SRLV infection of these cells [26]. Interestingly, 4-month-old granulomas induced by vaccine 1 had significantly higher expression of *MR*, indicating that macrophage polarization may be influenced by the time that has elapsed since vaccine injection and the type of vaccine. Furthermore, vaccine 1 also produced more granulomas with necrosis, and *MR* expression is known to be induced following cellular death, as this receptor is involved in immune clearance [57]. In our study, *MR* expression was not altered by SRLV infection, consistent with previous in-vitro observations [25]. However, we detected an upregulation of *A3Z1* expression in granulomas from infected sheep, which contradicts in-vitro findings [25]. Our result may be linked to indirect activation mechanisms that stimulate *APOBEC3* expression via lentiviral-induced signalling molecules, as reported in the target organs of feline immunodeficiency virus in cats [58].

5. Conclusion

The present study advances understanding of the pathogenesis of AlOOH-induced post-vaccination granulomas in sheep. Morphometry and cellular composition of ovine AlOOH-induced granulomas are influenced by different factors such as vaccine type, time since vaccine administration and potential SRLV infection. Further studies are needed to investigate whether macrophage polarization can influence SRLV replication or if SRLVs modulate the granuloma microenvironment.

Statement of author contributions

Ana Rodríguez-Largo: Conceptualization; Data curation; Investigation; Writing – original draft, review & editing. **Álex Gómez:** Methodology; Visualization; Writing – review & editing. **Estela Pérez:** Methodology; Writing – review & editing. **Irati Moncayola:** Investigation. **Lucia Biagini:** Investigation; Visualization; Writing – review & editing. **Giacomo Rossi:** Investigation; Data curation; Visualization; Writing – review & editing. **Ignacio de Blas:** Data curation; Formal analysis. **Antonio Fernández:** Data curation; Investigation; Writing – review & editing. **Marta Pérez:** Funding acquisition; Methodology; Supervision; Writing – review & editing. **Idoia Glaria:** Conceptualization; Investigation; Methodology; Writing – review & editing. **Ramsés Reina:** Funding acquisition; Investigation; Methodology; Supervision; Writing – review & editing. **Lluís Luján:** Conceptualization; Funding acquisition; Supervision; Writing – review & editing.

Declaration on use of generative AI or AI-assisted technologies in the writing process

The authors declared that no generative artificial intelligence (AI) or AI-assisted technologies were used in the writing of this manuscript.

Funding

This study was supported by the Spanish Ministry of Science, Innovation and Universities (RTI2018-096172-B-C33) and the Recognized Research Group of the Government of Aragón (A17_17R, Animal Health and Reproduction). A. Rodríguez-Largo was a PhD student funded by the Spanish Ministry of Science, Innovation and Universities (grant reference: FPU18/01674).

Acknowledgments

The authors acknowledge Livio Galosi, Subeide Mari, Valentina Grifantini, Rosario Puyó and Santiago Becerra for their technical support. We also acknowledge the use of Servicio General de Apoyo a la Investigación-SAI, Universidad de Zaragoza.

Declaration of competing interests

The authors declared no conflicts of interest in relation to the research, authorship or publication of this article.

Appendix A. Supplementary data

Supplementary data to this article can be found online at https://doi.org/10.1016/j.jcpa.2024.11.002.

References

[1] Garçon N, Friede M. Evolution of adjuvants across the centuries. In: Orenstein W, Offit P, Edwards KM, Plotkin SA, editors. Plotkin's vaccines. 7th ed. Philadelphia: Elsevier; 2018. 61–74.e4. https://doi.org/10.1016/B978-0-323-35761-6.00006-7.

[2] Lindblad EB. Aluminium adjuvants — in retrospect and prospect. Vaccine 2004;22:3658–68. https://doi.org/10.1016/j.vaccine.2004.03.032.

[3] HogenEsch H. Mechanism of immunopotentiation and safety of aluminum adjuvants. Front Immunol 2013;3:406. https://doi.org/10.3389/fimmu.2012.00406.

[4] Ulanova M, Tarkowski A, Hahn-Zoric M, Hanson LÅ. The common vaccine adjuvant aluminum hydroxide up-regulates accessory properties of human monocytes via an interleukin-4-dependent mechanism. Infect Immun 2001;69:1151–9. https://doi.org/10.1128/IAI.69.2.1151-1159.2001.

[5] Rimaniol AC, Gras G, Verdier F, Capel F, Grigoriev VB, Porcheray F, et al. Aluminum hydroxide adjuvant induces macrophage differentiation towards a specialized antigen-presenting cell type. Vaccine 2004;22:3127–35. https://doi.org/10.1016/j.vaccine.2004.01.061.

[6] Jacobson LS, Lima H, Goldberg MF, Gocheva V, Tsiperson V, Sutterwala FS, et al. Cathepsin-mediated necrosis controls the adaptive immune response by Th2 (T helper type 2)-associated adjuvants. J Biol Chem 2013;288:7481–91. https://doi.org/10.1074/jbc.M112.400655.

[7] Kool M, Soullié T, Van Nimwegen M, Willart MAM, Muskens F, Jung S, et al. Alum adjuvant boosts adaptive immunity by inducing uric acid and activating inflammatory dendritic cells. J Exp Med 2008;205:869–82. https://doi.org/10.1084/jem.20071087.

[8] Marichal T, Ohata K, Bedoret D, Mesnil C, Sabatel C, Kobiyama K, et al. DNA released from dying host cells mediates aluminum adjuvant activity. Nat Med 2011;17:996–1002. https://doi.org/10.1038/nm.2403.

[9] Seubert A, Monaci E, Pizza M, O'Hagan DT, Wack A. The adjuvants aluminum hydroxide and MF59 induce monocyte and granulocyte chemoattractants and enhance monocyte differentiation toward dendritic cells. J Immunol 2008;180:5402–12. https://doi.org/10.4049/jimmunol.180.8.5402.

[10] Khan Z, Combadière C, Authier FJ, Itier V, Lux F, Exley C, et al. Slow CCL2-dependent translocation of biopersistent particles from muscle to brain. BMC Med 2013;11:99. https://doi.org/10.1186/1741-7015-11-99.

[11] Crépeaux G, Eidi H, David MO, Baba-Amer Y, Tzavara E, Giros B, et al. Non-linear dose-response of aluminium hydroxide adjuvant particles: selective low dose neurotoxicity. Toxicology 2017;375:48–57. https://doi.org/10.1016/j.tox.2016.11.018.

[12] Ganter M. Veterinary consultancy and health schemes in sheep: experiences and reflections from a local German outlook. Small Rumin Res 2008;76:55–67. https://doi.org/10.1016/j.smallrumres.2007.12.023.

[13] Lacasta D, Ferrer LM, Ramos JJ, González JM, Ortín A, Fthenakis GC. Vaccination schedules in small ruminant farms. Vet Microbiol 2015;181:34–46. https://doi.org/10.1016/j.vetmic.2015.07.018.

[14] Asín J, Molín J, Pérez M, Pinczowski P, Gimeno M, Navascués N, et al. Granulomas following subcutaneous injection with aluminum adjuvant-containing products in sheep. Vet Pathol 2019;56:418–28. https://doi.org/10.1177/0300985818809142.

[15] de Miguel R, Asín J, Rodríguez-Largo A, Molín J, Echeverría I, de Andrés D, et al. Detection of aluminum in lumbar spinal cord of sheep subcutaneously inoculated with aluminum-hydroxide containing products. J Inorg Biochem 2020;204:110871. https://doi.org/10.1016/j.jinorgbio.2019.110871.

[16] Mantovani A, Biswas SK, Galdiero MR, Sica A, Locati M. Macrophage plasticity and polarization in tissue repair and remodelling. J Pathol 2013;229:176–85. https://doi.org/10.1002/path.4133.

[17] Gordon S. Alternative activation of macrophages. Nat Rev Immunol 2003;3:23–35. https://doi.org/10.1038/nri978.

[18] Sica A, Mantovani A. Macrophage plasticity and polarization: in vivo veritas. J Clin Invest 2012;122:787–95. https://doi.org/10.1172/JCI59643.

[19] Wang L, Hu S, Liu Q, Li Y, Xu L, Zhang Z, et al. Porcine alveolar macrophage polarization is involved in inhibition of porcine reproductive and respiratory syndrome virus (PRRSV) replication. J Vet Med Sci 2017;79:1906–15. https://doi.org/10.1292/jvms.17-0258.

[20] Burdo TH, Walker J, Williams KC. Macrophage polarization in AIDS: dynamic interface between anti-viral and anti-inflammatory macrophages during acute and chronic infection. J Clin Cell Immunol 2015;6:333.

[21] Crespo H, Bertolotti L, Juganaru M, Glaria I, De Andrés D, Amorena B, et al. Small ruminant macrophage polarization may play a pivotal role on lentiviral infection. Vet Res 2013;44:1–13. https://doi.org/10.1186/1297-9716-44-83.

[22] Cronan MR, Beerman RW, Rosenberg AF, Saelens JW, Johnson MG, Oehlers SH, et al. Macrophage epithelial reprogramming underlies mycobacterial granuloma formation and promotes infection. Immunity 2016;45:861–76. https://doi.org/10.1016/j.immuni.2016.09.014.

[23] Fernández M, Benavides J, Castaño P, Elguezabal N, Fuertes M, Muñoz M, et al. Macrophage subsets within granulomatous intestinal lesions in bovine paratuberculosis. Vet Pathol 2017;54:82–93. https://doi.org/10.1177/0300985816653794.

[24] Larenas-Muñoz F, Hamed MG, Ruedas-Torres I, María Sánchez-Carvajal J, Domínguez J, José Pallarés F, et al. Macrophage polarization in lymph node granulomas from cattle and pigs naturally infected with *Mycobacterium tuberculosis* complex. Vet Pathol 2024;61:792–802. https://doi.org/10.1177/03009858241231606.

[25] de Pablo-Maiso L, Glaria I, Crespo H, Nistal-Villán E, Andrésdóttir V, de Andrés D, et al. Characterization of ovine A3Z1 restriction properties against small ruminant lentiviruses (SRLVs). Viruses 2017;9:345. https://doi.org/10.3390/v9110345.

[26] Crespo H, Jauregui P, Glaria I, Sanjosé L, Polledo L, García-Marín JF, et al. Mannose receptor may be involved in small ruminant lentivirus pathogenesis. Vet Res 2012;43:43. https://doi.org/10.1186/1297-9716-43-43.

[27] Crespo H, Reina R, Glaria I, Ramírez H, de Andrés X, Jáuregui P, et al. Identification of the ovine mannose receptor and its possible role in visna/maedi virus infection. Vet Res 2011;42:28. https://doi.org/10.1186/1297-9716-42-28.

[28] Minguijón E, Reina R, Pérez M, Polledo L, Villoria M, Ramírez H, et al. Small ruminant lentivirus infections and diseases. Vet Microbiol 2015;181:75–89. https://doi.org/10.1016/j.vetmic.2015.08.007.

[29] Juste RA, Villoria M, Leginagoikoa I, Ugarte E, Minguijon E. Milk production losses in Latxa dairy sheep associated with small ruminant lentivirus infection. Prev Vet Med 2020;176. https://doi.org/10.1016/j.prevetmed.2020.104886.

[30] Echeverría I, De Miguel R, De Pablo-Maiso L, Glaria I, Benito AA, De Blas I, et al. Multi-platform detection of small ruminant lentivirus antibodies and provirus as biomarkers of production losses. Front Vet Sci 2020;7:182. https://doi.org/10.3389/fvets.2020.00182.

[31] Carrozza M-L, Niewiadomska A-M, Mazzei M, Abi-Said MR, Hué S, Hughes J, et al. Emergence and pandemic spread of small ruminant lentiviruses. Virus Evol 2023;9:vead005. https://doi.org/10.1093/ve/vead005.

[32] Blacklaws BA. Small ruminant lentiviruses: immunopathogenesis of visna-maedi and caprine arthritis and encephalitis virus. Comp Immunol Microbiol Infect Dis 2012;35:259–69. https://doi.org/10.1016/j.cimid.2011.12.003.

[33] Reina R, Andrés D, Amorena B. Immunization against small ruminant lentiviruses. Viruses 2013;5:1948–63. https://doi.org/10.3390/v5081948.

[34] Echeverría I, de Miguel R, Asín J, Rodríguez-Largo A, Fernández A, Pérez M, et al. Replication of small ruminant lentiviruses in aluminum hydroxide-induced granulomas in sheep: a potential new factor for viral dissemination. J Virol 2020;95:e01859. https://doi.org/10.1128/JVI.01859-20. 20.

[35] Rodríguez-Largo A, Castells E, de Miguel R, Gómez Á, Ruiz H, Pérez M, et al. Detection of aluminium hydroxide-induced granulomas in sheep by computed tomography: a feasible approach for small ruminant lentiviruses diagnosis and research. Vet Med Sci 2021;7:1757–61. https://doi.org/10.1002/VMS3.572.

[36] Pinczowski P, Sanjosé L, Gimeno M, Crespo H, Glaria I, Amorena B, et al. Small ruminant lentiviruses in sheep: pathology and tropism of 2 strains using the bone marrow route. Vet Pathol 2017;54:413–24. https://doi.org/10.1177/0300985816688742.

[37] Berndt BC. Ramanujan's notebooks. New York: Springer New York; 1989. https://doi.org/10.1007/978-1-4612-4530-8.

[38] Preziuso S, Taccini E, Rossi G, Renzoni G, Braca G. Experimental maedi visna virus infection in sheep: a morphological, immunohistochemical and PCR study after three years of infection. Eur J Histochem 2003;47:373–8.

[39] Gayo E, Polledo L, Balseiro A, Martínez CP, García Iglesias MJ, Preziuso S, et al. Inflammatory lesion patterns in target organs of visna/maedi in sheep and their significance in the pathogenesis and diagnosis of the infection. J Comp Pathol 2018;159:49–56. https://doi.org/10.1016/j.jcpa.2018.01.001.

[40] Gayo E, Polledo L, Magalde A, Balseiro A, García Iglesias MJ, Pérez Martínez C, et al. Characterization of minimal lesions related to the presence of visna/maedi virus in the mammary gland and milk of dairy sheep. BMC Vet Res 2019;15:109. https://doi.org/10.1186/s12917-019-1855-3.

[41] Pfaffl MW. Relative quantification. In: Dorak M, editor. Real-time PCR. 1st ed. London: Taylor & Francis; 2006. p. 63–82.

[42] Daniel WD, Cross CL. Biostatistics: a foundation for analysis in the health sciences. 11th ed. Ames: Wiley; 2019.

[43] Mchugh ML. The Chi-square test of independence. Lessons in biostatistics. Biochem Med 2013;23:143–52. https://doi.org/10.11613/BM.2013.018.

[44] Lu F, HogenEsch H. Kinetics of the inflammatory response following intramuscular injection of aluminum adjuvant. Vaccine 2013;31:3979–86. https://doi.org/10.1016/j.vaccine.2013.05.107.

[45] Flarend RE, Hem SL, White JL, Elmore D, Suckow MA, Rudy AC, et al. In vivo absorption of aluminium-containing vaccine adjuvants using 26Al. Vaccine 1997;15:1314–8. https://doi.org/10.1016/S0264-410X(97)00041-8.

[46] Mant A, Chinnery F, Elliott T, Williams AP. The pathway of cross-presentation is influenced by the particle size of phagocytosed antigen. Immunology 2012;136:163–75. https://doi.org/10.1111/j.1365-2567.2012.03558.x.

[47] Santagostino SF, Assenmacher C-A, Tarrant JC, Adedeji AO, Radaelli E. Mechanisms of regulated cell death: current perspectives. Vet Pathol 2021;58:596–623. https://doi.org/10.1177/03009858211005537.

[48] Wiener DJ. Histologic features of hair follicle neoplasms and cysts in dogs and cats: a diagnostic guide. J Vet Diagn Invest 2021;33:479–97. https://doi.org/10.1177/1040638721993565.

[49] Oz HH, Foil CS, Memon MA, Al-Bagdadi FK, Turk MA, Sims D. Follicular cysts in sheep. J Am Vet Med Assoc 1985;187:502–3.
[50] White CP. Experiments on cell proliferation and metaplasia. J Pathol Bacteriol 1910;14:450–62. https://doi.org/10.1002/path.1700140405.
[51] Hopkins JG, Weld JT, Huber WM. Cyst formation, acneform lesions and hair growth following intradermal injection of staphylococci in sensitized rabbits. J Invest Dermatol 1951;16:339–54. https://doi.org/10.1038/jid.1951.41.
[52] Schumacher HHA, Ahmad T. Epidermal inclusion cyst after Bacillus Calmette-Guérin vaccination. Plast Reconstr Surg 2005;115:1449–50. https://doi.org/10.1097/01.PRS.0000157643.45821.CC.
[53] Alvarez-Rubio FJ, Martínez-Ortega JI, Fernández-Reyna I. Bullous pilomatrixoma after COVID-19 vaccination. Cureus 2022;14:e32370. https://doi.org/10.7759/cureus.32370.
[54] Yang Z, Song F, Winters L, Zhong J. Development of pilomatrixoma at the vaccination site: a rare complication of COVID-19 vaccination – a case report. Am J Case Rep 2023;24:e942280. https://doi.org/10.12659/AJCR.942280.
[55] Jeon H, Jeong S-H, Dhong E-S, Han S-K. Pilomatricoma arising at an influenza vaccination site. Arch Plast Surg 2014;41:775–7. https://doi.org/10.5999/aps.2014.41.6.775.
[56] Aquilina S, Gatt P, Boffa MJ. Pilomatricoma arising at a BCG vaccination site. Clin Exp Dermatol 2006;31:296–7. https://doi.org/10.1111/j.1365-2230.2005.02016.x.
[57] Garcia-Aguilar T, Espinosa-Cueto P, Magallanes-Puebla A, Mancilla R. The mannose receptor is involved in the phagocytosis of mycobacteria-induced apoptotic cells. J Immunol Res 2016;2016:1–14. https://doi.org/10.1155/2016/3845247.
[58] Troyer RM, Malmberg JL, Zheng X, Miller C, MacMillan M, Sprague WS, et al. Expression of APOBEC3 lentiviral restriction factors in cats. Viruses 2019;11:831. https://doi.org/10.3390/v11090831.